Journal of Alloys and Compounds 509 (2011) 2530–2534

Contents lists available at ScienceDirect

Journal of Alloys and Compounds

journal homepage: www.elsevier.com/locate/jallcom

Thermally stimulated current analysis of $Zn_{1-x}Cd_xO$ alloy films

A. Senol Aybek[a,*], Nihal Baysal[b], Muhsin Zor[a], Evren Turan[a], Metin Kul[a]

[a] Department of Physics, Anadolu University, Eskişehir 26470, Turkey
[b] Kılıçoglu Anadolu High School, Eskişehir 26050, Turkey

ARTICLE INFO

Article history:
Received 16 July 2010
Received in revised form
10 November 2010
Accepted 12 November 2010
Available online 19 November 2010

Keywords:
Oxide materials
Alloy films
Thermal analysis
Trap parameters
Chemical synthesis
Electronic properties

ABSTRACT

We have studied the structural and electrical properties of $Zn_{1-x}Cd_xO$ alloy films deposited by ultrasonic spray pyrolysis technique. XRD measurement indicated that pure ZnO and CdO samples had single phases with hexagonal wurtzite and cubic structures, respectively. However, $Zn_{1-x}Cd_xO$ alloy films with $x = 0.59$ and 0.78 exhibited mixtures of a hexagonal wurtzite ZnO phase and a cubic CdO phase. Analysis of thermally stimulated current spectra of $Zn_{1-x}Cd_xO$ alloy films revealed the existence of a number of overlapped peaks each characterized by different trap energy levels located in the range of 0.033–0.215 eV below the conduction band. We have used curve fitting method for the evaluation of the trap parameters of the alloy films. The values of attempt-to-escape frequency ν, capture cross-section S and concentration of the traps N_t have been determined.

1. Introduction

There are quite number of transparent conducting oxides (TCO) of which the most commonly known ones are the binary systems, i.e. SnO_2, ZnO, In_2O_3, Ga_2O_3, and CdO [1–3]. The pure and mixed oxide alloy films of TCO materials are extensively studied. For different applications, different TCO materials may possess advantageous properties [4]. CdO and ZnO are both promising materials for their applications as window and buffer layers in thin film solar cells. CdO possesses cubic structure and a direct band gap of 2.3 eV, whereas ZnO is a wide band gap semiconducting oxide material ($E_g = 3.2$ eV) [5,6]. Hence, it is possible to modify the physical properties of ZnO upon mixing with CdO. Most of the recent works have been focused on the preparation of $Zn_{1-x}Cd_xO$ alloy films [7–9] and knowledge of the physical properties of these films is very limited [10]. $Zn_{1-x}Cd_xO$ alloy would be a good candidate because of the small direct band gap of CdO which shows a redshift of the luminescence peak with respect to that of ZnO [11].

Various techniques have been employed to prepare $Zn_{1-x}Cd_xO$ films such as dc reactive magnetron sputtering [12], thermal evaporation [8], metalorganic chemical vapour deposition [13], electrochemical deposition [14], pulsed laser deposition [15], sol–gel method [16] and ultrasonic spray pyrolysis [17]. Amongst all the deposition techniques, the USP is a versatile method for producing various materials in a wide range of composition, good thickness uniformity over a large area, homogeneous particle composition with controlled particle size [18]. In the ultrasonic spray pyrolysis process, ideal conditions of deposition are obtained when the droplet approaches the substrate just as the solvent is completely vaporized. The droplets of the solution generated by ultrasonic waves can be transported by the carrier gas to a heated surface of the substrate, where several reactions such as solvent evaporation and atomic rearrangement take place successively [19].

For the preparation of reproducible and reliable solar cells, it is important to control the electrical properties of $Zn_{1-x}Cd_xO$ layer. The photoconductivity and thermal conductivity of $Zn_{1-x}Cd_xO$ films are related to traps which are an individual impurity or defect in a crystal that affect the carrier transport properties. Therefore, it is important to get information about the activation energies of the trap levels in $Zn_{1-x}Cd_xO$ films. Some of the measurement methods widely used for the investigation of charge carrier traps in materials are thermoluminescence (TL) [20], thermally stimulated depolarization conductivity (TSDC) [21], and thermally stimulated current [22]. Among them, the TSC measurement is a well known non-isothermal technique for the investigation of trap levels in semiconducting materials. Many insulating, semi-insulating and semiconductor materials show thermally stimulated effects during heating [22]. In principle, this method consists in filling the traps after cooling down the material too low temperature and then heating the material at a constant rate and observing the thermally stimulated current as the traps are emptied. The energy level within

* Corresponding author. Tel.: +90 222 3350580; fax: +90 222 3204910.
E-mail address: saybek@anadolu.edu.tr (A.S. Aybek).

0925-8388/$ – see front matter © 2010 Elsevier B.V. All rights reserved.
doi:10.1016/j.jallcom.2010.11.077

the band gap of a particular trapping centre is related to the temperature at which it is emptied, while the number of traps contributing to the observed current peak depends on the amount of trapped charges, which are released [23]. The TSC permits a survey of the gap states and also the determination of the capture cross-section of each trap level [24].

The graph of current versus temperature is called the TSC curve. If the trapped charge carriers (electrons) thermally released to the conduction band on heating the material, the TSC would indicate a peak in the curve. This peak might well be a single peak which is favourable but rarely observed, or could be consisted of overlapping peaks. There are several methods to evaluate the trapping parameters from the experimental TSC spectra [22]. Of these, the curve fitting method has been widely used for the analysis of the TSC curves.

The subject of this work is to obtain more information concerning traps in $Zn_{1-x}Cd_xO$ alloy films by means of thermally stimulated current measurements in the temperature range of 40–300 K. The experimental data have been analyzed by using curve fitting method. The trap energy, the capture cross-section, the attempt-to-escape frequency and the concentration of the traps in $Zn_{1-x}Cd_xO$ films are reported.

2. Experimental details

$Zn_{1-x}Cd_xO$ alloy films have been deposited onto microscope glass substrates by the ultrasonic spray pyrolysis method at substrate temperatures of 325 °C for $x = 0$, 375 °C for $x = 0.59$ and 0.78, and 400 °C for $x = 1$. The apparatus of the deposition system used in this work are given elsewhere [25]. The substrates (11 mm × 13 mm × 1 mm) were soaked in acetone bath and washed in deionised water and dried in air. The aqueous 0.1 M of $Cd(CH_3COO)_2 \cdot 2H_2O$ and 0.1 M $ZnCl_2$ dissolved in deionised water were used to obtain $Zn_{1-x}Cd_xO$ samples. The prepared solutions were sprayed on the glass substrates through the spray head which contains 58 kHz transducer and the droplet sizes are between 30 and 60 μm. N_2 was used as a carrier gas with a pressure of 0.2 bar. The solution flow rate was kept constant at 2 ml/min. The ultrasonic spray head to substrate distance was approximately 40 cm.

Thicknesses of the samples were determined by weight difference method assuming the samples are uniform and dense as that of bulk having density of 8.15 g/cm^3 for CdO and 5.67 g/cm^3 for ZnO. The thicknesses of $Zn_{1-x}Cd_xO$ samples with different x values (0, 0.59, 0.78, and 1) were determined to be 630, 230, 330 and 550 nm, respectively. The crystal structure of the samples was analyzed by using Rigaku X-ray spectrophotometer with Cu Kα radiation (1.5406 Å).

The electrical measurement of the films was performed by means of the dc two-probe method. The metal contacts have been established by vacuum deposition of gold stripes of 4.5 mm separation and 3.5 mm in lengths. Copper wires have been attached to the gold contacts by small droplets of silver paste. The current–voltage (I–V) measurements are used for the determination of the conduction mechanism and the conductivity of the samples. Dark current–voltage measurements have been performed between 0.01 V and 100 V at room temperature.

The thermally stimulated current measurements (TSC) have been carried out in an Oxford Instruments 43305 Model closed-cycle helium gas cooling cryostat in the temperature range between 40 and 300 K. A vacuum of the order of 10^{-3} mbar is maintained throughout the measurements. The sample is cooled to an initial temperature of about 40 K and keeping it in dark for 30 min before starting illumination. The sample temperature has been measured by means of Chromel/Au–0.03%Fe/Chromel thermocouple. The sample has been illuminated for the generation of free carriers at 40 K for 15 min using a monochromatic UV light source of 18.2 mW/cm^2 with a wavelength of 365 nm. Following the termination of the illumination, the sample is heated up to room temperature with 0.12 K/s heating rate. The discharge current under an applied constant bias voltage of 10 V has been recorded as a function of temperature by using HP4140B pA meter/DC Voltage Source, Agilent 34401 Model Digital Multimeter, and VEE One Lab 6.1 computer program.

3. Results and discussion

3.1. Structural characteristics

The XRD patterns of $Zn_{1-x}Cd_xO$ thin films are shown in Fig. 1. The existence of multiple diffraction peaks indicate that the samples are polycrystalline in nature with hexagonal wurtzite structure for ZnO phases (JCPDS card no.: 036-1451) and cubic structure for CdO phases (JCPDS card no.: 05-0640). As shown in Fig. 1, X-ray characteristic peaks for ZnO are significantly reduced when the concentration of cadmium increases in the composition.

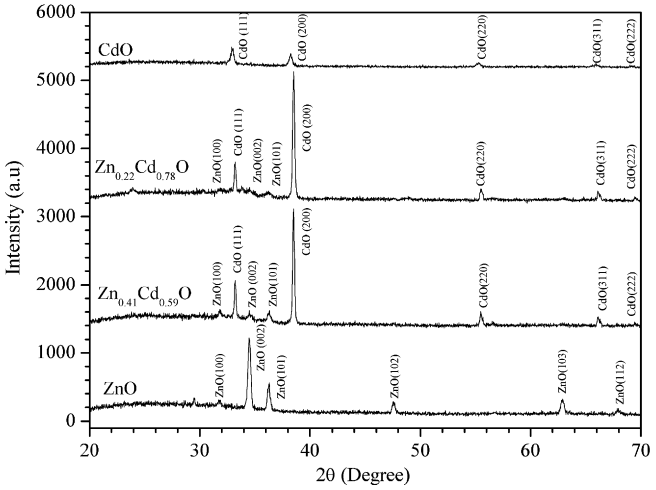

Fig. 1. X-ray diffraction patterns for $Zn_{1-x}Cd_xO$ films with different Cd contents.

Table 1
The lattice constants of $Zn_{1-x}Cd_xO$ alloy films.

Sample	Wurtzite ZnO			Cubic CdO
	a (Å)	c (Å)	c/a	a (Å)
ZnO	3.254	5.2128	1.602	
$Zn_{0.41}Cd_{0.59}O$	3.241	5.1986	1.604	4.6774
$Zn_{0.22}Cd_{0.78}O$	3.252	5.2004	1.599	4.6754
CdO				4.7086

The lattice parameters were calculated for the hexagonal and cubic structures respectively using the following equations which are given by [26]

$$\frac{1}{d_{hkl}^2} = \frac{4}{3}\left[\frac{h^2+hk+k^2}{a^2}\right] + \frac{l^2}{c^2} \quad \text{and} \quad \frac{1}{d_{hkl}^2} = \frac{h^2+k^2+l^2}{a^2} \tag{1}$$

where ($h\,k\,l$) are Miller indices of the plane, a and c are the lattice constants. The values of the lattice constants are given in Table 1. The c/a ratios for the samples are very close to the ideal value of 1.633 for wurtzite structure.

The crystallite size in $Zn_{1-x}Cd_xO$ alloy films were estimated from the half width at the maximum diffraction peak with the highest intensity by using the Scherrer formula [26].

$$D = \frac{0.9\lambda}{\beta \cos\theta} \tag{2}$$

where λ is the wavelength of X-ray, θ is the Bragg angle and β is the width of half maxima. The calculated values of the crystallite size are given in Table 2. It is seen that the crystallite size of ZnO decreases with increasing Cd content in the sample.

Table 2
The calculated values of the crystallite size of $Zn_{1-x}Cd_xO$ alloy films.

Crystallite size (nm)					
ZnO (0 0 2)	$Zn_{0.41}Cd_{0.59}O$		$Zn_{0.22}Cd_{0.78}O$		CdO (1 1 1)
	ZnO (1 0 1)	CdO (2 0 0)	ZnO (1 0 1)	CdO (2 0 0)	
35.5	33.9	59.1	24.5	47.9	54.9

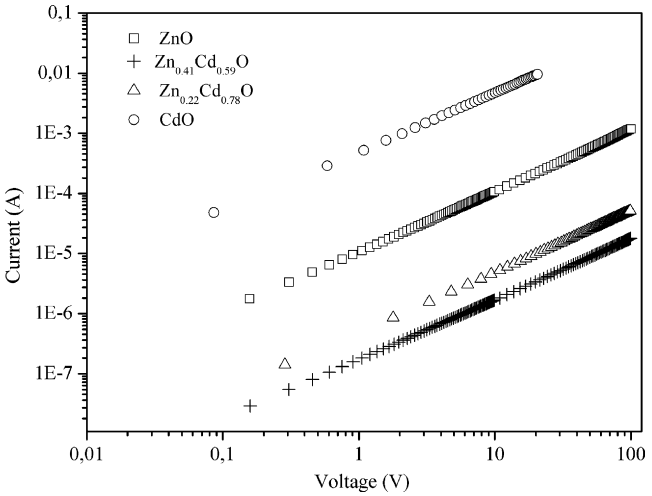

Fig. 2. The current–voltage characteristics of $Zn_{1-x}Cd_xO$ alloy films at room temperature in dark.

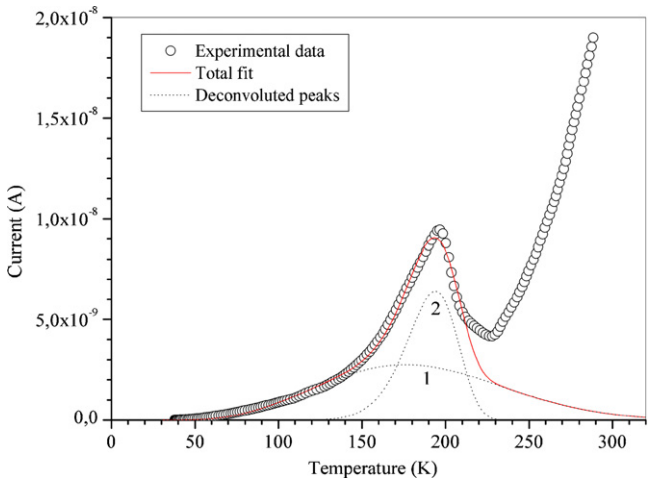

Fig. 3. The TSC analysis in the temperature range 40–300 K for ZnO film together with the numerical deconvolution of two components and the best fit.

3.2. Electrical properties

3.2.1. I–V characteristics

The electrical conductivity of the studied samples was n-type as determined by hot probe method. Fig. 2 presents the dark log–log plot of the current–voltage (I–V) characteristics of $Zn_{1-x}Cd_xO$ films at room temperature in the voltage range of 0.01–100 V. It is clearly seen that the current varies linearly with voltage with a slope of one which is indicating the ohmic behaviour of the conduction mechanism in planar Au–$Zn_{1-x}Cd_xO$–Au structure.

The electrical conductivity values of the samples have been determined from the I–V measurements to be 13, 0.89, 4.44, 426 $(\Omega\,m)^{-1}$ with different x values (0, 0.59, 0.78, and 1), respectively. The interesting point here is that the conductivities of the alloyed oxides seem to be noticeably decreased with respect to either CdO or ZnO. Although increasing Cd content in the alloy causes relevant increment in the conductivity but, it is still much lower than the conductivity of CdO. The plausible reason for the lower conductivity in the alloy oxides is that the existence of the interfacial potential barrier between both of the phases of CdO and ZnO present in the alloy with crystallite sizes of 59 and 34 nm, respectively. Assuming homogenous distribution of both phases the decrease in conductivity is thus expected due to the decrease in mobility of the carriers moving across the different phases [27]. Beside this, the effect of the alloy fluctuations on electron drift mobility would also be taken into account for further consideration for the low conductivity in $Zn_{1-x}Cd_xO$ alloy films [28].

3.2.2. Thermally stimulated currents

The thermally stimulated current data have been obtained in the temperature range 40–300 K with the heating rate of $\beta = 0.12$ K/s to evaluate the trapping parameters of the samples. Figs. 3 and 4 show the TSC spectra of ZnO and $Zn_{0.41}Cd_{0.59}O$ films. The TSC curves of $Zn_{1-x}Cd_xO$ films clearly show the existence of a number of overlapped peaks each characterized by a different trap energy level and attempt-to-escape frequency.

Calculating the trap parameters from TSC curves is the main goal of TSC theory. There are several methods in literature to evaluate the trapping parameters from experimental TSC curve namely as curve fitting, heating rates, and initial rise method. Many of them are based on the measurement of the maximum and the high and the low half-intensity temperatures [29]. However, the applicability of the many of methods is restricted for a TSC curve being complex due to the presence of a number of overlapped peaks. The curve fitting method appears to be more reliable because of using information from a broader range of the peak [30]. In this work, the experimental TSC curves for the samples have been analyzed by using the curve fitting method.

In the curve fitting method of determining the trapping parameters from an experimental curve, different equations are utilized depending on the recombination kinetics. The TSC curves of the samples studied in this work are composed of several peaks described by a main peak with a slight asymmetric rise on the low-temperature side as shown in Figs. 3 and 4. When the peak shape is examined (Fig. 5), we see that the "symmetry factor" μ_g ($=\delta/\omega$) becomes equal to 0.33 which is indicative of the slow retrapping [22]. Under monomolecular conditions (i.e. slow retrapping), the TSC curve of a discrete set of traps with a trapping level E_t below the conduction band is described by [31],

$$\sigma(T) = n_t \tau\, e\mu\nu \exp\left\{-\frac{E_t}{kT} - \int_{T_0}^{T} \frac{\nu}{\beta}\exp\left(-\frac{E_t}{kT}\right) dT\right\} \quad (3)$$

where σ is the thermally stimulated conductivity, n_t is the initial density of filled traps, τ is the lifetime of the free electron, e is the electronic charge, μ is the electron mobility, ν is the attempt-to-escape frequency of a trapped electron, β is the linear heating rate, k is the Boltzmann constant, T_0 is the initial temperature, and T is the temperature. The attempt-to-escape frequency ν depends on

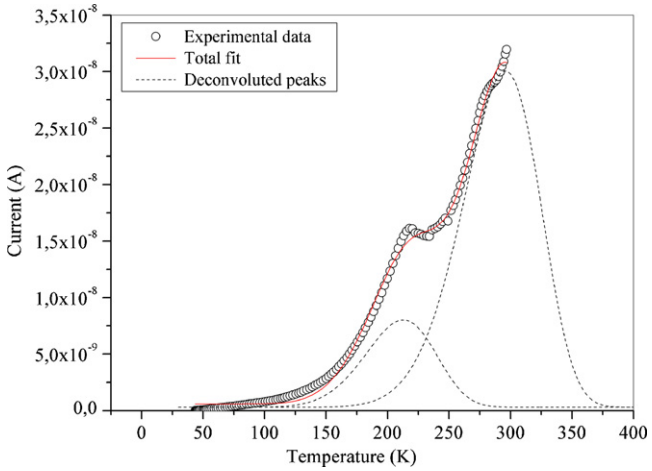

Fig. 4. Experimental TSC spectrum of $Zn_{0.41}Cd_{0.59}O$ alloy film and the deconvolution of the curve into two separate peaks using the curve fitting method.

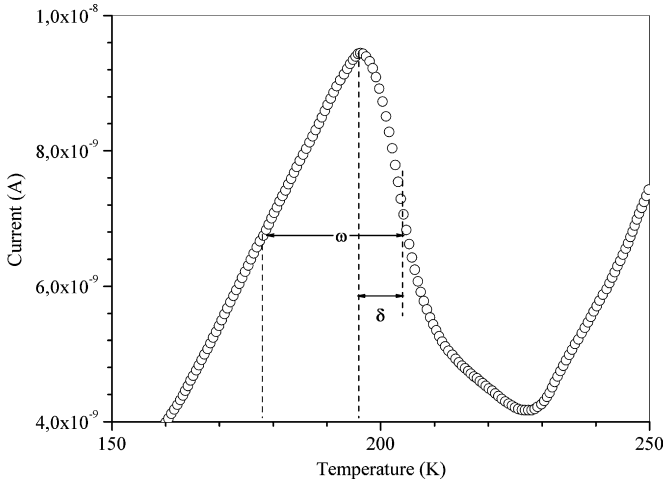

Fig. 5. Experimental asymmetric TSC curve with the parameters ω and δ of ZnO film.

temperature like T^a with $-2 \le a \le 2$ which is related to the dependence of the effective density of the states in the conduction band, N_c, and thermal velocity of free carriers, υ_{th} on temperature. This is a rather mild dependence on temperature as compared to the exponent $\exp(-E_t/kT)$ in Eq. (3), and can therefore be neglected as a first approximation [22]. If it is assumed that ν is independent of T and that over the temperature range of the TSC curve, the variation of μ and τ with T can be ignored, then for slow retrapping, $\sigma(T)$ can be rewritten as [29,32]

$$\sigma(T) = A \exp\left\{ -\frac{E_t}{kT} - \frac{\nu}{\beta} \int_{T_0}^{T} \exp\left(-\frac{E_t}{kT}\right) dT \right\} \quad (4)$$

where A is a constant, $\nu = SN_c\upsilon_{th}$, S is the capture cross-section of the trap, and $N_c = 2(2\pi m_e^* kT/h^2)^{3/2}$. Using the first term of the relevant asymptotic series for evaluating the integral, and putting $B = \nu E_t/\beta k$ and $t = E_t/kT$, Eq. (4) becomes

$$\sigma(T) = A \exp\{-t - B\exp(-t)t^{-2}\} \quad (5)$$

where B is a constant and can be approximated by

$$B \cong B' = \exp(t_m)\frac{t_m^3}{t_m + 2} \quad (6)$$

where $t_m = E_t/kT_m$ and T_m is the temperature at maximum intensity σ_m. By using B' instead of B, the free parameters become E_t and T_m instead of E_t and ν. This leads to a convenient method of the curve fitting, with only one variable parameter, E_t, since T_m is known experimentally.

In order to analyze all peaks of the TSC spectrum simultaneously, the fitting function consisting of the sum of all features of the TSC spectrum is described by [33]:

$$\sigma(T) = \sum_{i=1}^{m} \sigma_i(T) \quad (7)$$

In this equation, $\sigma_i(T)$ represents the current contribution of each peak, which is calculated from Eq. (5), and m is the number of the related peaks involved in the calculation.

The TSC spectra of ZnO and $Zn_{0.41}Cd_{0.59}O$ films have been fitted by means of a numerical procedure in order to distinguish the spectral components contributing to the signal and to determine the trap parameters. Accordingly the curve fitting is applied to the TSC curve for the analysis by using OriginPro 7.5 computer program. The program uses a Marquardt–Levenberg algorithm to minimize the difference between the experimental data and the fitting equation.

Table 3
Activation energy (E_t), capture cross-section (S), attempt-to-escape frequency (ν) and concentration of traps (N_t) for each TSC peaks of ZnO film and $Zn_{0.41}Cd_{0.59}O$ alloy film.

Sample	T_m (K)	E_t (eV)	ν (s^{-1})	S (m^2)	N_t (m^{-3})
ZnO	176	0.033	6.55×10^{-3}	2.70×10^{-32}	1.53×10^{20}
	194	0.197	0.83×10^{3}	2.81×10^{-27}	4.42×10^{19}
$Zn_{0.41}Cd_{0.59}O$	213	0.118	1.67	3.15×10^{-30}	9.77×10^{19}
	296	0.215	12.52	1.22×10^{-29}	9.56×10^{19}

Following the curve fitting method, we have obtained two main deconvoluted peaks of which one of them is wide indicated as 1 in Fig. 3 and the other is narrow indicated as 2. The wider one expands from about 50 K to above about 300 K. It is hardly acceptable to assume that this peak corresponds to a single level trap. It is, in this case, quite possible to assume that this peak might have been composed of the several trap distributions in the band gap [22]. Once the curve had been fitted and the final values of the trap energies below the conduction band and T_m for each peak were determined in ZnO and $Zn_{0.41}Cd_{0.59}O$ films as given in Table 3, then Eq. (5) was used to calculate B and hence the attempt-to-escape frequency ν. Knowing the value of ν, we have calculated the capture cross-section S for each trap level. Since this equation contains the effective density of states in the conduction band, the value of the electron effective mass is required for ZnO and $Zn_{0.41}Cd_{0.59}O$ films. Therefore, we have used the value of $0.24m_0$ for ZnO film with wurtzite structure [34]. The electron effective mass of $Zn_{0.41}Cd_{0.59}O$ sample was determined to be $0.36m_0$ by means of a linear extrapolation of the electron effective mass values [28] for the wurtzite phase with $m^*(ZnO) = 0.24m_0$ and for the cubic phase with $m^*(CdO) = 0.44m_0$ [35]. The values of the attempt-to-escape frequency ν and the capture cross-section S calculated from the curve fitting results are also given in Table 3. It can be noticed that the values of the attempt-to-escape frequency are by far lower than usually expected those of less than 10^{12} 1/s [22]. The reasonable explanation for low values of the attempt-to-escape frequency is probably related to the peak obtained by the deconvolution which may be consisted of several peaks that suggests a strong repulsive barrier to capture the carriers [36]. The capture cross-sections of the traps present in the samples were calculated in the range 2.70×10^{-32}–2.81×10^{-27} m^2.

The concentration of the traps was estimated from the area under the TSC curve corresponding to that trap using the relation [27]:

$$N_t = \frac{1}{eG^*V} \int J_{TSC} dt \quad (8)$$

where e is the electronic charge, G^* is the photoconductivity gain and V is the sample volume, and J_{TSC} is the thermally stimulated current density. A reasonable approximation for G^* can be obtained by measuring the photon flux Φ needed to produce a photocurrent equal to the J_{TSC} at T_m of TSC maximum [27]:

$$G^* = \frac{J_{\max}}{e\Phi} \quad (9)$$

where J_{max} is the maximum TSC. The values of N_t obtained for the traps in ZnO and $Zn_{0.41}Cd_{0.59}O$ films are also presented in Table 3.

The experimental TSC results indicate that polycrystalline ZnO and $Zn_{0.41}Cd_{0.59}O$ films exhibit the high concentration trap characteristics located in the range of 0.033–0.215 eV below the conduction band. It appears that the observed trap levels may be due to a large number of defects and/or impurities that act as electronic trapping sites in $Zn_{1-x}Cd_xO$ films. Although it is difficult to identify the defects associated with these trapping levels, the experimental findings reported here could be assigned below.

In the samples that we have examined, shallow trap energy of 0.033 eV dominates at low temperatures, although various deeper traps are also present when approaching to higher temperatures. As seen in Fig. 3, two overlapped peaks were registered at levels of 0.033 and 0.197 eV in ZnO sample. According to the literature [37–39], it has long been assumed that two most common defects in ZnO films are oxygen vacancies (V_O) and zinc interstitials (Zn_i) as the dominant donor since most ZnO material is strongly n-type. It is also suggested that Zn_i rather than V_O is the dominant native shallow donor in ZnO with activation energy of about 0.03–0.05 eV [38–40]. The observed trap energy level of 0.033 eV in the TSC spectrum of ZnO sample is thought to originate from zinc interstitials which is attributed to the donor-like trap. In the literature, oxygen vacancy levels in ZnO are reported in the range of 0.050 eV and nearly 1 eV [41–46]. The trap energy of 0.197 eV in this study is within the range of the values in the literature. This observed trap energy level could most likely be attributed to the oxygen vacancy which can be also found in ZnO films.

Evaluation of the TSC curve for $Zn_{0.41}Cd_{0.59}O$ alloy film revealed two peaks at temperatures 213 and 296 K after the deconvolution of the TSC spectrum by the curve fitting technique as shown in Fig. 4. The incorporation of Cd into $Zn_{1-x}Cd_xO$ films with $x = 0.59$ have resulted in vanishing the trap level at 0.033 eV which is present in the ZnO film (Fig. 3). The trapping levels observed at 0.118 and 0.215 eV in $Zn_{0.41}Cd_{0.59}O$ alloy film are almost coincident with those of ZnO sample. Thereby, possible origins of the traps with activation energy of 0.118 and 0.215 eV are also related to oxygen vacancies in $Zn_{0.41}Cd_{0.59}O$ alloy film.

In addition to the above-mentioned possible origin of the trap levels in $Zn_{1-x}Cd_xO$ films, it is also generally accepted that oxygen plays a crucial role as trapping centers either at the surface or at the grain boundaries where it can easily be adsorbed [47,48]. Therefore, the observed trap energies of 0.033 eV and 0.118–0.215 eV in $Zn_{1-x}Cd_xO$ films could be considered due to the adsorbed oxygen at the film surface and the adsorbed oxygen at the grain boundaries in the lattice, respectively [49,50].

4. Conclusions

$Zn_{1-x}Cd_xO$ films have been produced onto microscope glass substrates by the ultrasonic spray pyrolysis method. The samples are polycrystalline with hexagonal wurtzite structure for ZnO and cubic structure for CdO film, while the films with $x = 0.59$ and 0.78 are mixtures of a hexagonal wurtzite ZnO phase and a cubic CdO phase.

Ohmic mechanism has been determined from the current–voltage relationship. The electrical conductivity values of $Zn_{1-x}Cd_xO$ alloy films have been calculated to be 13, 0.89, 4.44, 426 $(\Omega\,m)^{-1}$ with different x values (0, 0.59, 0.78, and 1), respectively. The incorporation of the Cd into $Zn_{1-x}Cd_xO$ films with $x = 0.59$ causes a significant decrease in the conductivity as compared with pure ZnO and pure CdO.

The effect of the Cd incorporation into ZnO material on trapping levels was investigated by the TSC measurements. Two overlapped peaks were registered at levels of 0.033 and 0.197 eV in ZnO sample by the curve fitting technique. The observed trap energy levels for ZnO film is thought to originate from zinc interstitials and oxygen vacancies. However, the incorporation of Cd into $Zn_{1-x}Cd_xO$ alloy films with $x = 0.59$ have resulted in two trapping centers with activation energies of 0.118 and 0.215 eV. The observed trap levels in $Zn_{0.41}Cd_{0.59}O$ alloy film are related to oxygen adsorption in the sample. Attempt-to-escape frequency, concentration and capture cross-section of the traps were calculated from the curve fitting results. The smaller value of the attempt to escape frequency might well be due to the imperfect state of the sample and also observed in some other samples [51–53].

Acknowledgment

This work was supported by Scientific Research Fund, Anadolu University, under Grant No. O11056.

References

[1] M. Batzill, U. Diebold, Prog. Surf. Sci. 79 (2005) 47–154.
[2] K.L. Chopra, S. Major, D.K. Pandya, Thin Solid Films 102 (1983) 1–46.
[3] T.J. Coutts, D.L. Young, X. Li, MRS Bull. 25 (2000) 58–65.
[4] R.G. Gordon, MRS Bull. 25 (2000) 52–57.
[5] C.Y. Liu, Y.C. Liu, J. Alloys Compd. 482 (2009) 393–395.
[6] P. Fons, K. Iwata, S. Niki, A. Yamada, K. Matsubara, M. Watanabe, J. Cryst. Growth 209 (2000) 532–536.
[7] W.E. Mahmoud, A.A. Al-Ghamdi, F. El-Tantawy, S. Al-Heniti, J. Alloys Compd. 485 (2009) 59–63.
[8] F. Wang, B. Liu, C. Zhao, S. Yuan, Mater. Lett. 63 (2009) 1357–1359.
[9] G. Li, X. Wang, Y. Wang, X. Shi, N. Yao, B. Zhang, Physica E 40 (2008) 2649–2653.
[10] S. Vijayalakshmi, S. Venkataraj, R. Jayavel, J. Phys. D: Appl. Phys. 41 (2008) 245403–245409.
[11] M.D. Uplane, P.N. Kshirsagan, B.J. Lokhande, C.H. Bhosale, Mater. Chem. Phys. 64 (2000) 75–78.
[12] G.D. Yuan, Z.Z. Ye, J.Y. Huang, L.P. Zhu, Solid State Commun. 149 (2009) 290–292.
[13] J. Ishihara, A. Nakamura, S. Shigemori, T. Aoki, J. Temmyo, Appl. Surf. Sci. 244 (2005) 381–384.
[14] G. Li, W. Zhao, Q. Bu, Y. Tong, Electrochem. Commun. 11 (2009) 282–285.
[15] P. Misra, P.K. Sahoo, P. Tripathi, V.N. Kulkarni, R.V. Nandedkar, L.M. Kukreja, Appl. Phys. A 78 (2004) 37–40.
[16] Y.S. Choi, C.G. Lee, S.M. Cho, Thin Solid Films 289 (1996) 153–158.
[17] A.S. Aybek, N. Baysal, M. Zor, E. Turan, M. Kul, Thin Solid Films 515 (2007) 8709–8713.
[18] Y. Wang, W. Chen, Q. Luo, S. Xie, C.H. Chen, Appl. Surf. Sci. 252 (2006) 8096–8101.
[19] K.Y. Choi, K.D. Kim, J.W. Yang, J. Mater. Process. Technol. 171 (2006) 118–124.
[20] C.H. Lee, S.K. Kim, H.Y. Du, G.N. Jeon, J. Phys. D: Appl. Phys. 24 (1991) 422–427.
[21] S.W.S. McKeever, E. Lilley, J. Phys. C: Solid State Phys. 14 (1981) 3547–3555.
[22] R. Chen, Y. Kirsh, Analysis of Thermally Stimulated Processes, Pergamon, Oxford, 1981.
[23] G. Micocci, A. Tepore, J. Appl. Phys. 80 (1996) 894–897.
[24] R.H. Bube, Photoconductivity of Solids, Wiley, New York, 1960.
[25] M. Kul, M. Zor, A.S. Aybek, S. Irmak, E. Turan, Sol. Energy Mater. Sol. Cells 91 (2007) 882–887.
[26] B.D. Cullity, S.R. Stock, Elements of X-ray Diffraction, Prentice-Hall, Upper Saddle River, NJ, 2001.
[27] R.H. Bube, Photoelectronic Properties of Semiconductors, Cambridge University Press, England, 1992.
[28] B.K. Ridley, Phys. Status Solidi A 176 (1999) 359–362.
[29] N.S. Mohan, R. Chen, J. Phys. D: Appl. Phys. 3 (1970) 243–247.
[30] R. Chen, Surf. Sci. 400 (1998) 258–265.
[31] R.R. Hearing, E.N. Adams, Phys. Rev. 117 (1960) 451–454.
[32] T.A.T. Cowell, J. Woods, Br. J. Appl. Phys. 18 (1967) 1045–1051.
[33] L. Pintilie, I. Pintilie, D. Petre, T. Botila, M. Alexe, Appl. Phys. A 69 (1999) 105–109.
[34] F. Benharrats, K. Zitouni, A. Kadri, B. Gil, Superlattices Microstruct. 47 (2010) 592–596.
[35] K. Gurumurugan, D. Mangalaraj, S.K. Narayandass, K. Sekar, C.P. Girija Vallabhan, Semicond. Sci. Technol. 9 (1994) 1827–1832.
[36] D.C. Look, Z.Q. Fang, W. Kim, O. Aktas, A. Botchkarev, A. Salvador, H. Morkoc, Appl. Phys. Lett. 63 (1996) 3775–3777.
[37] C. Casteleiro, H.L. Gomes, P. Stallinga, L. Bentes, R. Ayouchi, R. Schwarz, J. Non-Cryst. Solids 354 (2008) 2519–2522.
[38] Ü. Özgür, Ya.I. Alivov, C. Liu, A. Teke, M.A. Reshchikov, S. Doğan, V. Avrutin, S.J. Cho, H. Morkoç, J. Appl. Phys. 98 (2005) 041301–041404.
[39] D.C. Look, J.W. Hemsky, J.R. Sizelove, Phys. Rev. Lett. 82 (1999) 2552–2555.
[40] H. Von Wenckstern, H. Schmidt, M. Grundmann, M.W. Allen, P. Miller, R.J. Reeves, S.M. Durbin, Appl. Phys. Lett. 91 (2007) 022913–022915.
[41] D.C. Look, D.C. Reynolds, C.R. Sizelove, R.L. Jones, C.W. Litton, G. Cantwell, W.C. Harsch, Solid State Commun. 105 (1998) 399–401.
[42] C.G. Van de Walle, Physica B 308–310 (2001) 899–903.
[43] A. Janotti, C.G. Van de Walle, Appl. Phys. Lett. 87 (2005) 122102.
[44] F. Tuomisto, K. Saarine, D.C. Look, G.C. Farlow, Phys. Rev. B 72 (2005) 085206.
[45] T. Frank, G. Pensl, R. Tena-Zaera, J. Zuniga-Perez, C. Martinez-Tomas, V. Munoz-Sanjose, T. Ohshima, H. Itoh, D. Hofmann, D. Pfisterer, J. Sann, B. Meyer, Appl. Phys. A 88 (2007) 141–145.
[46] Z.-Q. Fang, B. Claflin, D.C. Look, G.C. Farlow, J. Appl. Phys. 101 (2007) 086106.
[47] K.S. Ramaiah, J. Mater. Sci.: Mater. Electron 10 (1999) 291–294.
[48] D. Petre, I. Pintilie, E. Pentia, I. Pintilie, T. Botila, Mater. Sci. Eng. B 58 (1999) 238–243.
[49] E. Turan, M. Zor, A.S. Aybek, M. Kul, Physica B 395 (2007) 57–64.
[50] A.S. Aybek, M. Kul, E. Turan, M. Zor, E. Gedik, J. Phys.: Condens. Matter 20 (2008) 055216–055220.
[51] I. Guler, N.M. Gasanly, Solid State Commun. 150 (2010) 176–180.
[52] I. Guler, N.M. Gasanly, J. Alloys Compd. 485 (2009) 41–45.
[53] T. Yildirim, N.M. Gasanly, Curr. Appl. Phys. 9 (2009) 1278–1282.